# THE ATLANTIC-WIDE RESEARCH PROGRAMME FOR BLUEFIN TUNA (GBYP Phase 10)

SHORT-TERM CONTRACT (ICCAT GBYP 04/2021)

**Model-based inference to estimate density and abundance of bluefin tuna: feasibility study**

**Final Report**

15 September 2021


**CREEM, University of St Andrews**

L Burt, M Chudzinska, D Miller, D Borchers and S Buckland



This project is co-funded by the European Union

Please cite this report as: Burt *et al.* (2021) Model-based inference to estimate density and abundance of bluefin tuna: feasibility study. Report number CREEM-2021-04. Provided to ICCAT, September 2021 (Unpublished).

## Document control

Please consider this document as uncontrolled copy when printed.

| Version | Date | Reason for issue | Prepared by | Checked by |
|---|---|---|---|---|
| DRAFT v1 | 22/06/2021 | Outline of report | LB | MC |
| DRAFT v4 | 28/07/2021 | Review by co-authors | LB | MC |
| DRAFT v10 | 27/08/2021 | Implement multi-step modelling | LB MC DM | DB SB |
| DRAFT v15 | 10/09/2021 | Corrections | LB | MC DLB SB |

The University of St Andrews is a charity registered in Scotland No. SCO13532.

# SUMMARY

Information was required on the distribution, biomass and abundance of spawning stock (adult individuals) of bluefin tuna in the Mediterranean Sea. Aerial surveys took place between late May and early August in years 2010-2011, 2013, 2015, 2017-2019 in four spawning regions of the Mediterranean Sea. Planes flew along predetermined track lines and trained observers searched for groups of tuna, recording the group size, biomass and other relevant information on the environmental conditions. A total of 146,782 km were covered on search effort during 210 days of surveys resulting in 317 sightings. Line transect distance sampling methods (Buckland *et al.*, 2001) were applied to the data collected on these surveys to estimate tuna abundance (Chudzinska *et al.*, 2021). These design-based DS methods estimated average density in each block and each year.

Model-based methods (e.g. Hedley and Buckland, 2004) allow density and abundance to be estimated as a function of location and environment, allowing density to vary spatially throughout a region. This report applied such an approach to the aerial survey data collected in block A for the years 2017 to 2019. The objective was to assess the feasibility of using model-based methods to estimate tuna abundance for the other survey blocks, or indeed for the region of the Mediterranean covered by aerial surveys.

Two models were fitted, one to describe the number of groups and the other to describe group size. To illustrate this approach a limited set of potential explanatory variables were used, such as sea surface temperature on the day of the survey, sea surface temperature 10 days before and depth. Year and location were, however, important predictors in the fitted models. The selected models explained only small fractions of variation in density of groups and group sizes and there are large uncertainties around the estimated values. These data present challenges for modellers and further analyses, including more environmental covariates, are needed.

# INTRODUCTION

Aerial surveys have been undertaken in the Mediterranean for six years within the period 2011 to 2019, inclusive. The data collected during these surveys have been used to estimate abundance and biomass of blue fin tuna (BFT) using distance sampling (DS) methods (Buckland *et al.* 2001); details of this analysis is described in Chudzinska *et al.* (2021). DS methods estimate average density of animals within the region of interest but in reality, it is likely that density changes in response to environmental conditions and location. Model-based methods (Hedley and Buckland, 2004) estimate density which can vary in response to location/habitat and so predictions can be made based on the model and values of variables included in the model. The predicted surface may indicate regions of higher and lower density. If density is estimated to be high on the edges of the block, this may indicate that a substantial fraction of the population of interest is outside the block. If this was to occur, a revision of the survey region may be required to more fully capture the population.

In this report, model-based methods are implemented on a subset of the aerial survey data to assess their feasibility for application to the full dataset in future.

The data selected for this scoping study were from surveys in 2017, 2018 and 2019 in survey block A due to the uniform search protocol used in this period and block, as well as temporal overlap between the presence of the spawning stock and survey time.

# SURVEY DATA

The extent of the region of interest is shown in Figure 1; this included the extent of block A in 2019 and the overlap regions in other years (for details see Fig 1.2 Cañadas A and Vázquez, 2020). The total area of this region was $7.1448 \times 10^4$ km$^2$ (Figure 1). [1]

Transects were aligned approximately north to south within the survey block.

Surveys were undertaken in May and June (Table 1). Observers searched for marine fauna and, on sighting an animal, recorded the species, declination angle to the group, group size, biomass of the group and other pertinent information.

Table 1: Temporal distribution of survey effort.

| Year | Month | NumberDays |
|---|---|---:|
| 2017 | 05 | 2 |
| 2017 | 06 | 15 |
| 2018 | 05 | 1 |
| 2018 | 06 | 17 |
| 2019 | 05 | 3 |
| 2019 | 06 | 14 |

# STATISTICAL METHODS

The count method of Hedley and Buckland (2004) was implemented to model the trend in spatial distribution in BFT. A common approach is to model the number of individuals in a small section of effort as a function of location and environmental. However, due to the nature of these data, where the range of group size can

[1] The size of the region used in Chudzinska *et al.*, (2021) was 61,837km$^2$.

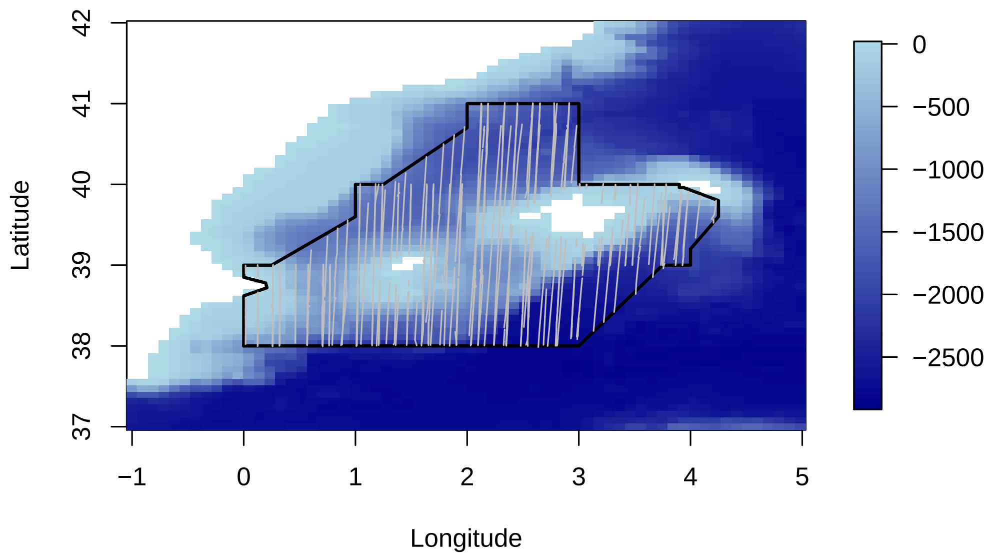


Figure 1: Survey region (black line), transects (grey lines) and depth (metres).

be from few to thousands (1 - 3000 individuals in the data used in this model), a multi-step process was implemented:

- a model was fitted to the number of BFT groups ("group encounter rate model")
- a model was fitted to group size ("group size model")
- predictions from these two models were multiplied to produce a surface of BFT abundance.

## Modelling the number of groups

The response variable was the estimated number of groups in a small section (segment) $i$ of track line (of length $l_i$), $\hat{n}_i$, calculated using a Horvitz-Thompson-type estimator (Horvitz and Thompson, 1952) as follows:

$$\hat{n}_i = \sum_{r=1}^{R_i} \frac{1}{\hat{p}_r}$$

where $R_i$ is the number of detected groups in segment $i$. The parameter $\hat{p}_r$ is the estimated probability of detection for group $r$ in segment $i$; this was estimated using distance sampling (DS) methods (Buckland *et al.*, 2001) (see below for details).

The lengths of track lines were calculated from the recorded positions (i.e. latitude and longitude), when observers were on search effort. In addition, only groups sighted when observers were on search effort were included in the analysis. The target length of segments was 10 km but segments varied from this because of breaks in search effort.

### Probability of detection

The critical assumptions of DS methods are that all groups on the transect (i.e., at zero perpendicular distance) are detected with certainty, groups are detected at their initial location and that distance measurements are exact. Given these assumptions, the distribution of perpendicular distances was used to model how the probability of detection decreased with increasing distance from the transect line.

The probability of detection was estimated from a detection function model fitted to the observed distribution of perpendicular distances using exact distances. Perpendicular distances were truncated at 1,500 m to avoid a long tail in the detection function. Following Chudzinska *et al.* (2021), a half-normal detection function was fitted with log(group size) as an explanatory variable. Only one company (Airmed) surveyed block A in the years 2017-2019 and so 'Company', used by Chudzinska *et al.* (2021), was not included in the detection function. The models were fitted in R (R Core Team 2019) using the `Distance` package (Miller *et al.*, 2019b).

### Model specification

The estimated numbers of BFT groups per segment along the transect lines were used to estimate group abundance in the region of interest. This approach models trend in the density and allows it to vary throughout the region of interest.

The number of groups in each segment (with known area) was estimated, $\hat{n}_i$ where $i$ indicates an individual segment, and this formed the response variable in the statistical model.

Counts are often modelled using a Poisson distribution, however, these data were over dispersed (i.e. more variable than expected for Poisson distributed data), and, therefore, we assumed a Tweedie distribution, which allows a bit more flexibility, for the counts.

The mean ($\mu_i$) was modelled with location, habitat and temporal variables as candidate explanatory variables represented as follows.

$$\mu_i = \exp(\log_e(a_i) + \beta_0 + \sum_j^J \beta_j F_{ij} + \sum_k^K s_k(D_{ik}) + s_l(X_i, Y_i))$$

where

- $\log_e(a_i)$ is an offset term (a term with known regression coefficient) that corresponds to the area of each segment ($a_i = 2wl_i$ where $w$ is the strip width and $l_i$ is the length of each segment $i$),
- $\beta_0$ is an intercept,
- $\beta_j F_{ij}$ represent factor terms (e.g. year) with $\beta_j$ representing the regression coefficients for jth factor variable,
- $s_k(D_{ik})$ represent one dimensional smooth terms (e.g. depth)
- $s_l(x_i, y_i)$ represents a two-dimensional smooth term of location (determined for each segment $i$ by $X_i$ and $Y_i$).

The models were fitted using generalised additive models in the R package `dsm` (Miller *et al.*, 2013; Miller *et al.*, 2019a).

### Candidate explanatory variables

The available candidate explanatory variables were:

- year (*year*, as a factor with 3 levels),

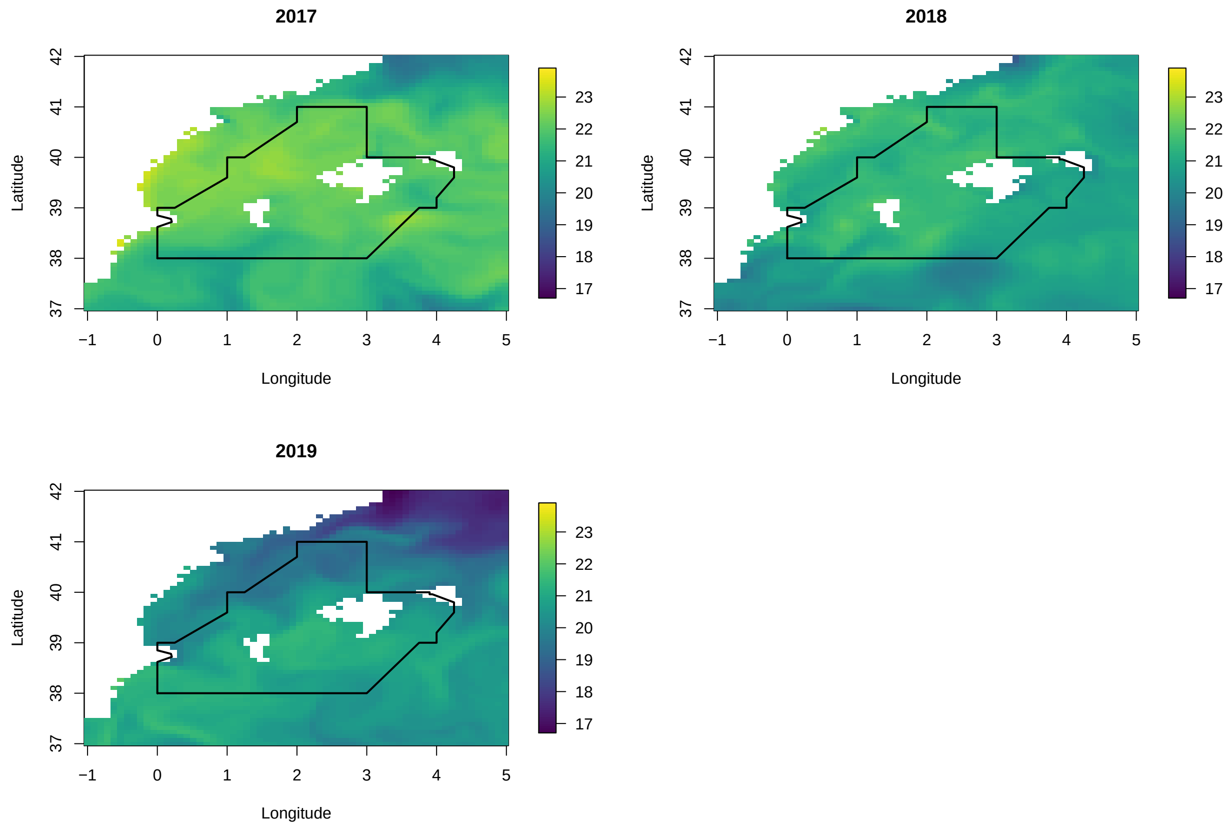


Figure 2: Sea surface temperatures ($^o$C) on 10 June in 2017, 2018 and 2019, representing midpoints of the three surveys.

- location of the segment ($x, y$; as kilometres from a reference point to the midpoint of the segment), fitted as a 2-dimensional term and also as a 3-dimensional term with $year$,
- depth in metres ($depth$), fitted as a 1-dimensional term,
- daily sea surface temperature ($SST$) for the day of the survey, fitted as a 1-dimensional term,
- $SST$ for 10 days prior to the survey date ($SST10$) , fitted as a 1-dimensional term.

Longitude and latitude were transformed into a distance (in km) east ($x$) and north ($y$), respectively, from a reference point in the survey region (1$^o$W, 37$^o$N). This was to ensure that a unit change in the north-south direction was the same as a unit change in the east-west direction. Location is unlikely to determine BFT distribution but it acts as a proxy for other unmeasured or unknown variables that will determine BFT distribution.

Depth was obtained from ETOPO1, a 1-arc-minute global relief model (https://www.ngdc.noaa.gov/mgg/global/global.html).

$SST$ and $SST10$ were obtained from Copernicus (www.copernicus.eu) and provided by ICCAT (Figure 2).

The group encounter rate model included an interaction between location and the factor $year$ such that there was a separate smooth for each factor level with the same smoothing parameter for all smooths (using the option `bs="fs"`).

$SST$ and $SST10$ were correlated (see later) and are also associated with day of year, hence, only one of these terms was included in a model with the other available variables. These one-dimensional terms were fitted with a modification to the smoothing penalty such that the term could effectively be excluded (i.e. the argument `bs="ts"` was included in the model specification) (Pedersen *et al.*, 2019). Having determined which of these candidate variables explained the most variation in the response, the model was examined and terms removed if necessary.

### Modelling group sizes

In this step, only sightings data were included and the response variable in the generalized additive model (GAM) was recorded group size; this was modelled as a function of the candidate variables described above. Since a group of size zero is impossible, a potentially useful distribution to describe these data is the zero-truncated Poisson, possibly including overdispersion. However in practice, specifying these distributions created errors in the model fitting and so after some trial and error, the square root of the group sizes were modelled as a normal distribution (even though this is not theoretically correct).

Term selection started by including all candidate variables in the model ("full model") and model reduction was based on effective degrees of freedom (edf), variables with edf $< 1$ were removed from the model ("shrinkage method"). Two full models were tested: one including location and year as interaction and one without any interactions. Model checking was based on setting basis size (i.e. $k$), quantile-quantile (q-q) plots, and looking at residuals. Comparison between final candidate models was based on AIC, deviance explained, and goodness of fit. The restricted maximum likelihood smoothing parameter estimation method was used for all models.

The models were fitted in the R package called `mgcv` (Wood, 2017).

### Estimating density and abundance

Using the selected model, predicted density of groups was calculated for a grid of points (the prediction grid) from the encounter rate model, with associated area and known values for the explanatory variables. We chose 10th of June as prediction day as it was a midpoint of the survey for all three years (see Figure 2). Similarly, group size was predicted over the same grid using the group size model. The two surfaces were then multiplied together resulting in the estimated number of individuals per cell.

Total abundance for the block was estimated by summing predicted number of individuals over all grid points in the region of interest (i.e. the area bounded by the black line in Figure 1). An average estimated group size in the region of interest was obtained from the average of the predicted group sizes in the block.

Uncertainty in the abundance estimate was obtained by combining uncertainty from GAM parameters, the detection function parameters and the group size model. We obtained this for the two GAM-based models via posterior simulation (Wood, 2017) by repeatedly sampling possible predictive surfaces from the encounter rate and group size models and taking their product for each cell, thus summary statistics over the samples (variances, etc.) encapsulate the model-based uncertainty from each model. In our final estimates of uncertainty, we also included uncertainty from the detection function via the delta method (summing squared coefficients of variation (CV)). This assumed independence between the spatial processes and the detection processes, but as there was little spatial pattern in group size and that was the only covariate in the detection function, this seems to be justifiable. Confidence intervals (CI) for abundance were obtained using log-normal 95% CI (Buckland *et al.*, 2001).

## RESULTS

### Search effort and numbers of groups detected

During the three years of surveys in block A, a total of $1.6589 \times 10^4$ km of search effort were flown and 71 groups of BFT were detected (Table 2). Group sizes ranged from 1 to 5000 taking into account all sightings

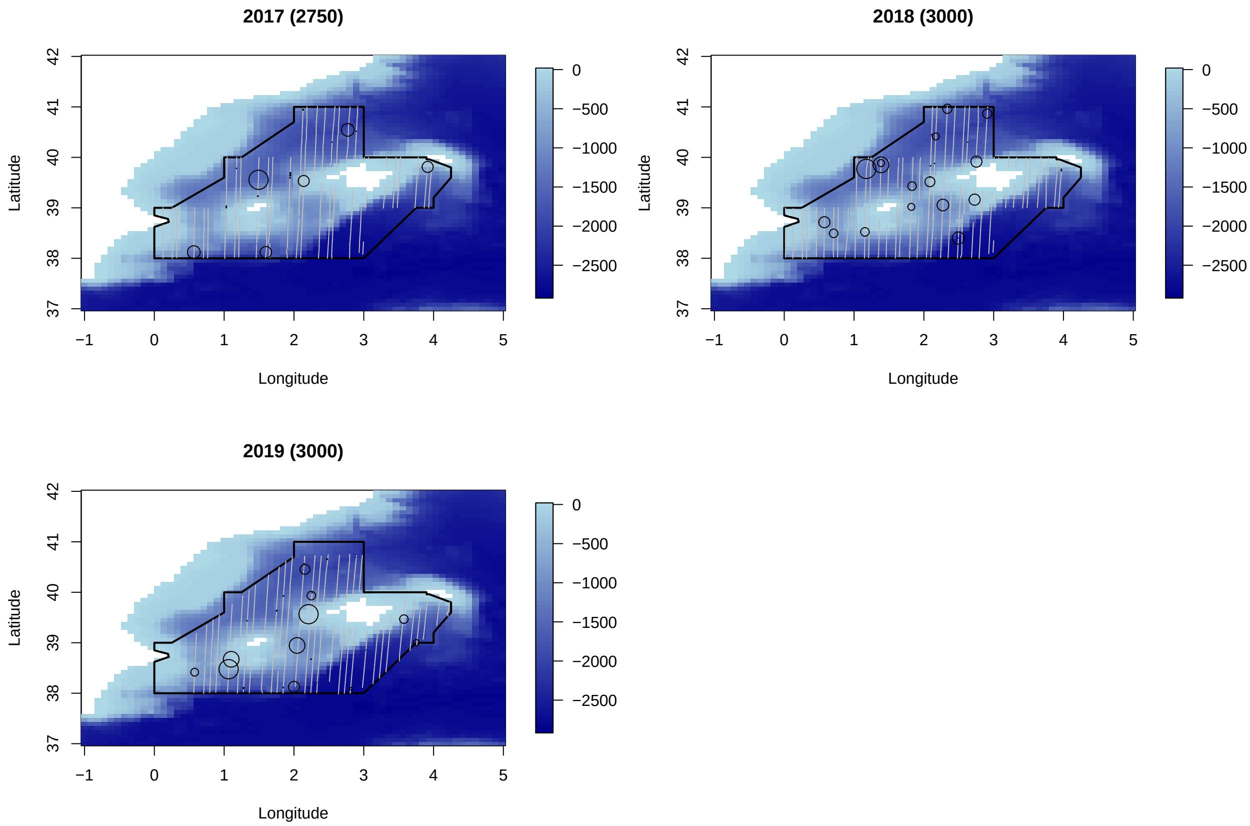


Figure 3: Location of search effort (lines) and (truncated) sighted groups (circles) overlaid on depth (metres). The area of the circle is proportional to the size of the sighted group; maximum group size given in parentheses.

(i.e. without truncation) (see below).

Table 2: Summary of survey effort and the number of groups detected and mean group size. The groups have not been truncated.

| Year | Effort | Number.Groups | Mean.Group.Size |
|---|---|---|---|
| 2017 | 4982 | 22 | 754 |
| 2018 | 6147 | 29 | 928 |
| 2019 | 5460 | 20 | 694 |

To fit the detection function, sighted groups were truncated at a perpendicular distance of 1,500 m leaving 62 groups as described in Chudzinska *et al.*, (2021); the majority of groups were detected in the shallower waters in the region (Figure 3).

## Probability of detection

The detection function fitted to these data used a half-normal key function and included log(group size) as a covariate. The average probability of detection (over all group sizes) for the selected detection function was 0.21 (CV=0.14) (Figure 4).

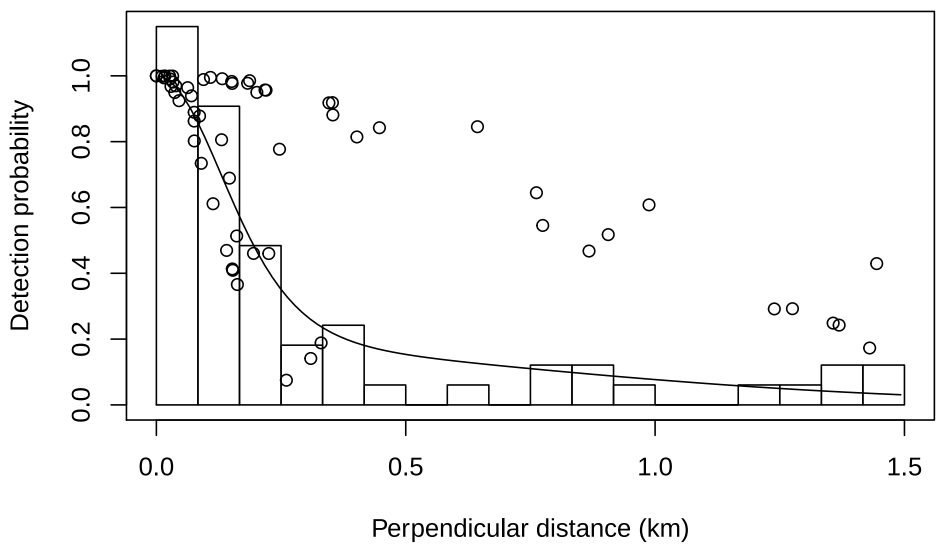


Figure 4: Estimated detection function (averaged over group size) overlaid onto the scaled distribution of perpendicular distances. Dots indicate individual values.

## Model selection

The data consisted of 1,899 segments (5 segments with missing covariates and one very small segment were removed before model fitting) and the average length was 8.7 km (range 0.12 - 14.9 km); 57 segments (3%) contained sightings.

Given the time of year of the surveys, $SST$ was slightly higher than $SST10$ and, not surprisingly, $SST$ was highly correlated with $SST10$ (correlation coefficient was 0.9) (Figure 5).

The variables included in both types of models (with group sizes and estimated number of groups as responses) and the deviances explained are shown in Table 3. See Appendix A for model diagnostics of the selected models (selected models are marked in bold capitals in Table 3).

Table 3: Summary of the fitted models. SST: sea surface temperature on a day of survey, SST10: SST 10 days before, YearF: year of survey as a factor. The numbers by each term indicate effective degrees of freedom. Models marked in bold capitals are the final models used to estimate density and abundance. Note, YearF is included as a factor in the models described as `No Interaction`.

| Number | Response | Description | Terms | Deviance | AIC |
|---|---|---|---|---|---|
| 1 | Group size | `Year-location interaction` | s(x,y,YearF, 2.3), s(SST10, 5.4e-05), s(depth, 0.56) | 12.05 | 532.88 |
| 2 | Group size | `Year-location interaction` | s(x,y,YearF, 3.1), s(SST, 0.72), s(depth, 0.54) | 18.38 | 532.51 |
| 3 | **GROUP SIZE** | `No interaction` | s(x,y, 0.91), s(SST, 0.82), s(depth, 0.52) | 17.65 | 530.19 |
| 4 | Group size | `No interaction` | s(x,y, 1), s(SST, 0.81) | 15.70 | 530.27 |

| Number | Response | Description | Terms | Deviance | AIC |
|---|---|---|---|---|---|
| 1 | Group encounter | `Year-location interaction` | s(x,y,YearF, 4.2), s(SST10, 8.8e-05), s(depth, 5.1e-05) | 8.05 | 2180.52 |
| 2 | Group encounter | `Year-location interaction` | s(x,y,YearF, 4.2), s(SST, 4.9e-05), s(depth, 0.00037) | 8.05 | 2180.52 |
| 3 | **GROUP EN-COUNTER** | `Year-location interaction` | s(x,y,YearF, 4.2) | 8.05 | 2180.52 |

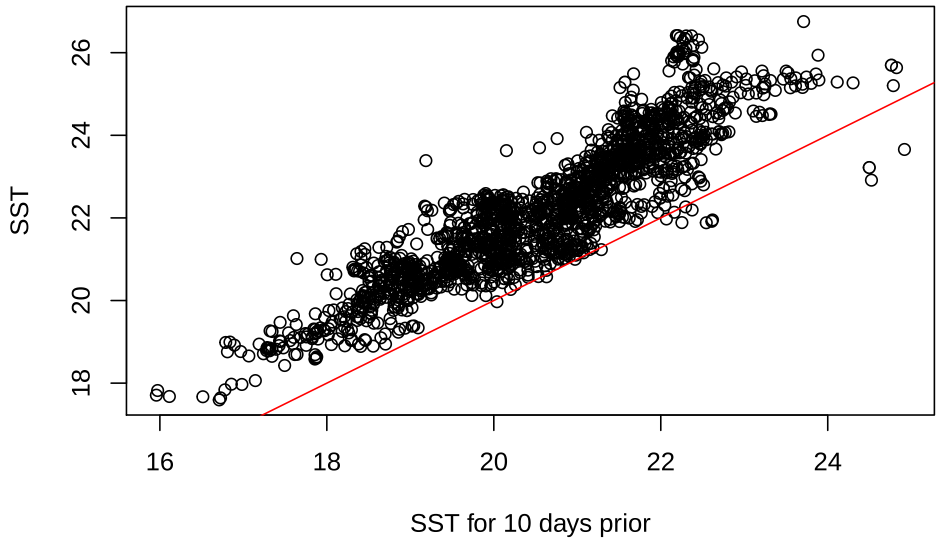


Figure 5: Comparison between $SST$ and $SST10$; the red line is a line of equality.

## Estimated density and abundance

The estimated abundances in the survey region for 10 June 2017, 2018 and 2019 are shown in Table 4.

Table 4: Model-based estimates of BFT in block A: number of groups and CV (CV.Groups), average group size and CV (CV.Group.Sizes), abundance and CV and 95% CI.

| Year | Groups | CV.Groups | Group.Size | CV.Group.Sizes | Abundance | CV | Lower.CI | Upper.CI |
|---|---|---|---|---|---|---|---|---|
| 2017 | 577 | 0.27 | 103 | 0.67 | 61925 | 0.74 | 17038 | 225067 |
| 2018 | 505 | 0.25 | 351 | 0.37 | 155540 | 0.46 | 65461 | 369575 |
| 2019 | 444 | 0.25 | 298 | 0.40 | 128368 | 0.49 | 51292 | 321268 |

Estimated density for each year is shown in Figure 6; only values in block A are shown in the plots below to highlight the pattern (see Figure B1 for estimated values outside block A). Higher densities were estimated in the eastern part of the region in 2017 and 2019 and in the north of the region in 2018. There are also large CVs associated with density (Figure 7) and abundance estimates (Table 4) and large CVs outside block A. The largest component of this CV is due to the uncertainty in the group sizes. See Appendix B for further details of the estimated number of groups and estimated group sizes.

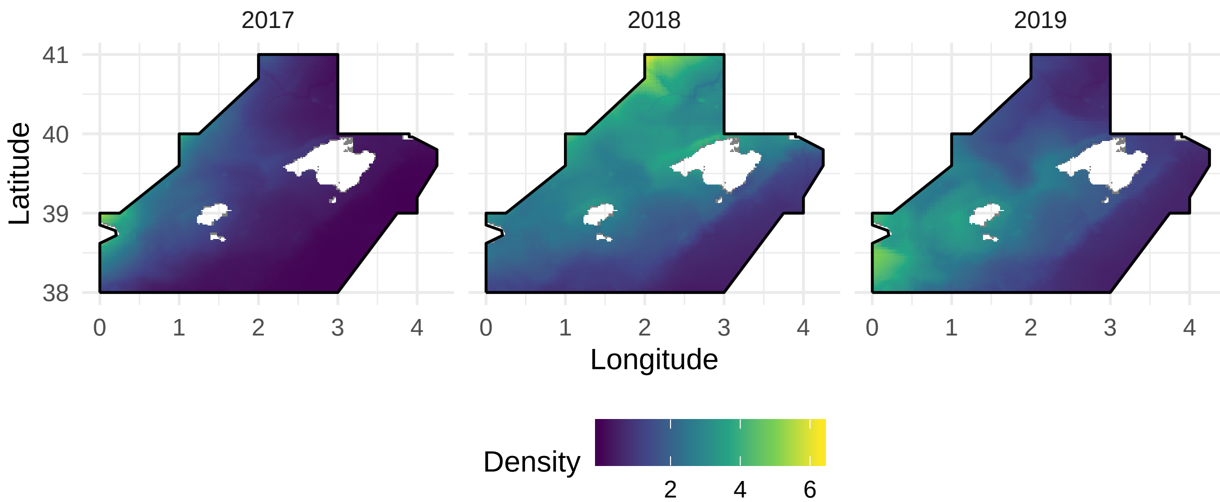


Figure 6: Estimated density of BFT (fish/km$^2$) for 10th June in 2017, 2018 and 2019.

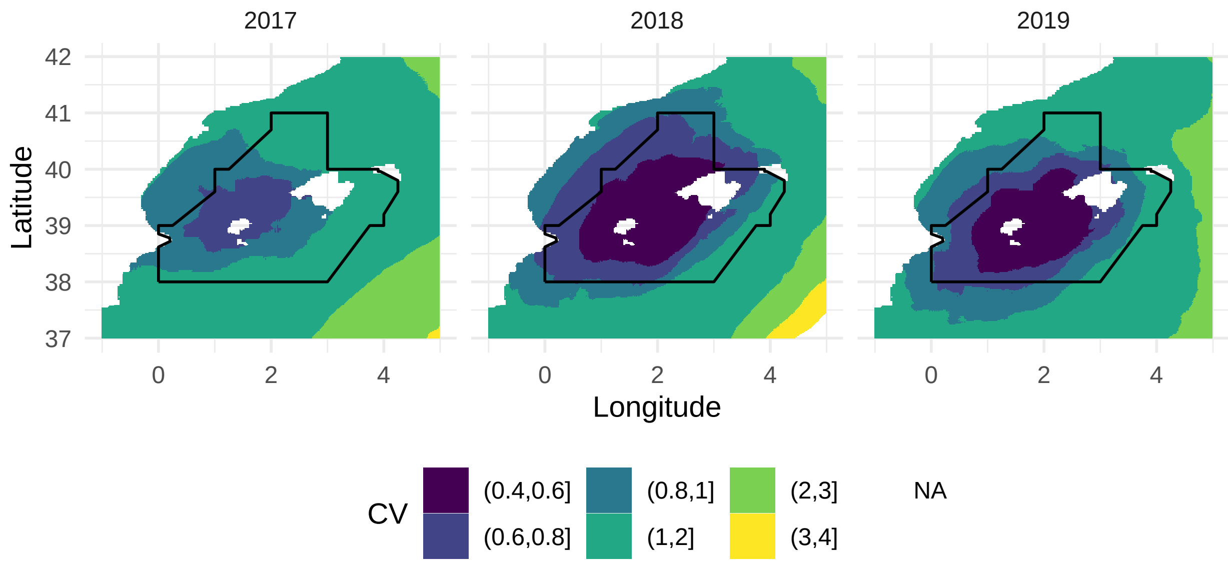


Figure 7: Coefficient of variation associated with density of BFT (not including detection function uncertainty).

# DISCUSSION

The presented report is a demonstration of using model-based inference to estimate density and abundance of BFT. We limited the data to one survey block and used a limited selection of potential explanatory variables: location, depth, $SST$ for the day of survey and 10 days prior. The distribution of BFT is, most likely, affected by a range of other environmental variables (e.g. distance to frontal systems, salinity) which can easily be included in the models in the future. The need to consider other variables is reflected in relatively low deviance explained by the models developed here (Table 3). (However, information on variables throughout the region of interest would be required for prediction).

The modelling was limited to data from one survey block in which data had been recorded most consistently for all surveys. However, these data have a number of characteristics which make modelling challenging:

- the majority of segments did not contain any sightings (hence the response value is zero)
- although the number of groups sighted was small, the range of group sizes was very large.

To deal with these issues a multi-step process was implemented so that, rather than using the estimated number of individuals in a segment as the response, the estimated number of groups was used. To convert groups to individuals, an estimate of group size was required and so group sizes were modelled separately. This part of the modelling was particularly challenging as the range of observed groups was very large. The selected model does not conform to all assumptions of the GAM, as highlighted in the q-q plots. Additional environmental and protocol-related covariates should, therefore, be taken into account in the future.

For this feasibility study, only a limited amount of model selection was performed and it is likely that other distributions may be more appropriate than the ones used here.

One aspect of this type of modelling is that it allows for prediction outside the region of interest, although caution needs to be exercised when considering prediction beyond the range of the observed data. Estimated densities for the full region are shown in Appendix B, Figure B1. High densities were estimated outside block A and may require further investigation.

The trend predictions in abundance for block A based on design-based DS methods from Chudzinska *et al.* 2021) are given in Table 5. These estimates were based on fitting a detection function to data for all blocks and the region used for prediction was smaller (61,837 km$^2$) than the one used here.

Table 5: Design-based estimates of BFT in block A taken from Chudzinska et al. (2021): expected group size, abundance, CV and 95% CI. The area of the region was 61,837 km$^2$.

| Year | Group.Size | Abundance | CV | Lower.CI | Upper.CI |
|---|---|---|---|---|---|
| 2017 | 115 | 49920 | 0.44 | 21820 | 114200 |
| 2018 | 239 | 81600 | 0.31 | 45280 | 147100 |
| 2019 | 229 | 75020 | 0.38 | 36710 | 153300 |

For a direct comparison between design-based and model-based estimates, design-based estimates were obtained using only the data used in the modelling presented here and for a region of size 71,448 km$^2$ (Table 6). The two sets of design-based estimates are very similar.

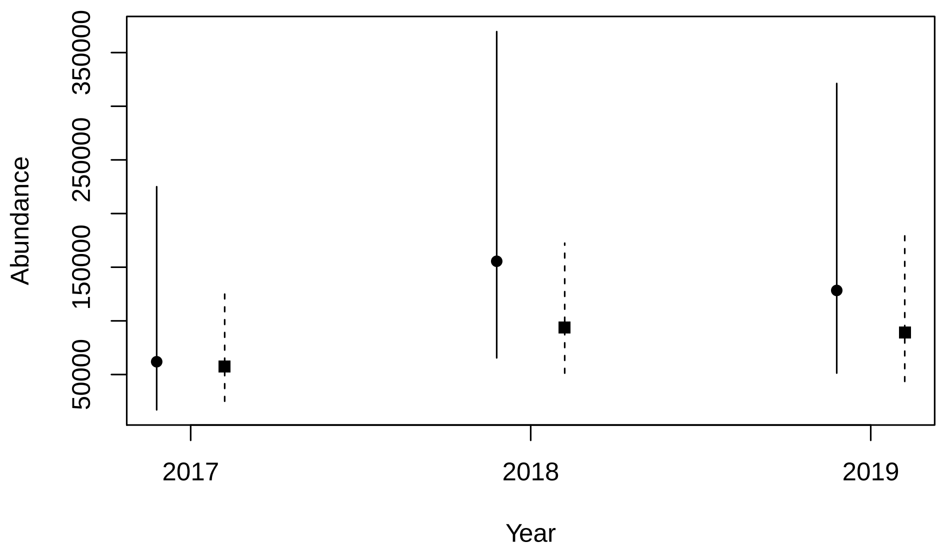


Figure 8: Comparison of model-based (dots and solid lines) and design-based (squares and dashed lines) abundance estimates and CIs.

Table 6: Design-based estimates of BFT using only data in block A: Number of groups and CV (CV.Groups), average group size and CV (CV.Group.Sizes), abundance of fish and CV and lower and upper 95% CI of abundance. The area of the region was 71,448 km$^2$.

| Year | Groups | CV.Groups | Group.Size | CV.Group.Size | Abundance | CV | Lower.CI | Upper.CI |
|---|---|---|---|---|---|---|---|---|
| 2017 | 504 | 0.35 | 114 | 0.53 | 57608 | 0.44 | 25061 | 132423 |
| 2018 | 396 | 0.32 | 237 | 0.40 | 94005 | 0.32 | 51242 | 172456 |
| 2019 | 392 | 0.30 | 227 | 0.44 | 88949 | 0.38 | 43536 | 181733 |

The numbers of groups from the model-based approach are slightly higher than for the design-based approach and also group sizes are higher, except for 2017. Nevertheless, the model-based estimates (Table 4) are within the 95% CI of the design-based estimates (Figure 8). Both approaches also indicate highest abundance in 2018 and lowest in 2017. The uncertainty is lower with the design-based estimates but, as with the model-based approach, the uncertainty associated with the group sizes is higher than the uncertainty associated with the number of groups.

One additional point to note is that in the design-based estimates, the CVs for group size are higher than the CVs for total abundance (Table 6). This suggests that group size and group density maybe negatively correlated (i.e. group size decreases as group density increases). The model-based method does not have this negative correlation built into it, and model-based estimates with lower CVs might be obtained were it built in. This requires further investigation.

# CONCLUSIONS

In the analysis presented here, a model-based approach was used to estimate BFT abundance in one survey block.

- These data were challenging to model due to the low number of sightings and the large variation in observed group sizes. To alleviate these problems, a multi-step modelling approach was implemented; a model was fitted to the estimated number of groups and to group sizes. Predicted values from these two models were multiplied to estimate number of individuals. Other possible approaches may consider fitting presence/absence of groups and then combining with estimated number of groups and group size.
- A limited selection of explanatory variables were used in this analysis but this method has potential to include more to understand the drivers of BFT density.
- Rather than using temperature variables directly, the difference in temperature between time points could be used.
- Including data from other survey blocks (C, E and G) and years would increase the number of sightings, however, the analysis is still likely to be challenging due to various issues related to data collection in the other regions, such as temporal mismatch between survey and spawning season, unstandarised survey protocols between years and regions.
- Prediction outside the survey block is of interest to inform the location of large spawning groups. The results indicated high density outside the survey block but this may indicate an extrapolation (i.e. predicting beyond the range of observed values or for a combination of values not observed). Tools have recently been developed to inform the extrapolation of predictive models outside the range of the data (Bouchet *et al.*, 2020) and maybe of use in this application.

# ACKNOWLEDGEMENTS

This work has been carried out under the ICCAT Atlantic-Wide Research Programme for Bluefin Tuna (GBYP), which is funded by the European Union, several ICCAT CPCs, the ICCAT Secretariat, and other entities (see https://www.iccat.int/gbyp/en/overview.asp). The content of this paper does not necessarily reflect ICCAT's point of view or that of any of the other sponsors, who carry no responsibility. In addition, it does not indicate the Commission's future policy in this area.

We would like to thank Alfonso Pagá, Ana Cañadas and José Antonio Vázquez, for providing data, advice and expertise. Environmental data selection, compilation and formatting has been provided by D. Alvarez-Berastegui (IEO) and P. Tugores (SOCIB) in the framework of the PANDORA project (H2020, Grant Agreement No 773713), and the Bluefin tuna project.

# REFERENCES

Bouchet PJ, Miller DL, Roberts JJ, Mannocci L, Harris CM and Thomas L (2020) Extrapolation tools for density surface models. Methods in Ecology and Evolution. DOI: 10.1111/2041-210X.13469

Buckland ST, Anderson DR, Burnham KP, Laake JL, Borchers DL and Thomas L (2001) Introduction to distance sampling. Oxford University Press

Cañadas A, Vázquez A (2020) 2010-2019 Aerial Survey Data Re-Analysis. SHORT-TERM CONTRACT ICCAT GBYP 07/2019 Final report

Chudzinska M, Burt ML, Borchers D, Miller D, Buckland S (2021) ICCAT Bluefin Tuna Abundance and Biomass Estimates. Reanalysis of 2010-2019 Aerial Survey.Report number CREEM-2021-03. Unpublished report to ICCAT

Hedley SL and Buckland ST (2004) Spatial models for line transect sampling. Journal of Agricultural, Biological and Environmental Statistics 9:181-199

Horvitz D and Thompson D (1952) A Generalization of Sampling Without Replacement from a Finite Universe. Journal of the American Statistical Association, 47

Miller DL, Burt L, Rexstad E and Thomas L (2013) Spatial models for distance sampling data: Recent developments and future directions. Methods in Ecology and Evolution, 4:1001-1010

Miller DL, Rexstad E, Burt L, Bravington MV and Hedley S (2019a). dsm: Density Surface Modelling of Distance Sampling Data. R package version 2.2.18. http://github.com/DistanceDevelopment/dsm

Miller DL, Rexstad E, Thomas L, Marshall L and Laake JL (2019b) Distance Sampling in R. Journal of Statistical Software, 89(1):1-28. doi: 10.18637/jss.v089.i01 (URL: https://doi.org/10.18637/jss.v089.i01)

Pedersen E, Miller DL, Simpson GL and Ross N (2019) Hierarchical generalized additive models in ecology: an introduction with mgcv. PeerJ 7:e6876

R Core Team (2019) R: A language and environment for statistical computing. R Foundation for Statistical Computing, Vienna, Austria. URL https://www.R-project.org/

Wood SN (2017) Generalized Additive Models: An Introduction with R (2nd edition). Chapman and Hall/CRC

# Appendix A: Model summary and diagnostics

## Summary output for the group size model

```
##
## Family: gaussian
## Link function: identity
##
## Formula:
## sqrtsize ~ s(x, y, bs = "ts") + YearF + s(SST, bs = "ts") + s(depth,
##     bs = "ts")
##
## Parametric coefficients:
##             Estimate Std. Error t value Pr(>|t|)
## (Intercept)   10.014      4.138   2.420   0.0187 *
## YearF2018     10.751      5.322   2.020   0.0481 *
## YearF2019     10.736      6.061   1.771   0.0819 .
## ---
## Signif. codes:  0 '***' 0.001 '**' 0.01 '*' 0.05 '.' 0.1 ' ' 1
##
## Approximate significance of smooth terms:
##             edf Ref.df     F p-value
## s(x,y)   0.9120     29 0.071   0.110
## s(SST)   0.8194      9 0.429   0.030 *
## s(depth) 0.5220      9 0.119   0.155
## ---
## Signif. codes:  0 '***' 0.001 '**' 0.01 '*' 0.05 '.' 0.1 ' ' 1
##
## R-sq.(adj) =  0.115   Deviance explained = 17.6%
## -REML = 254.42  Scale est. = 262.75    n = 62
```

The plots below show the quantile-quantile plots (q-q plots) for all the fitted GAMs; ‘Inter’ indicates models where location was interacting with year, ‘No inter’ indicates models without any interaction included. Ideally, the residual q-q plots should lie on a straight line and the figure below shows that there is some deviation. Grey shaded areas show results of 100 replicates. The number in the plot caption is the model number (see Table 3); model number 3 was selected.

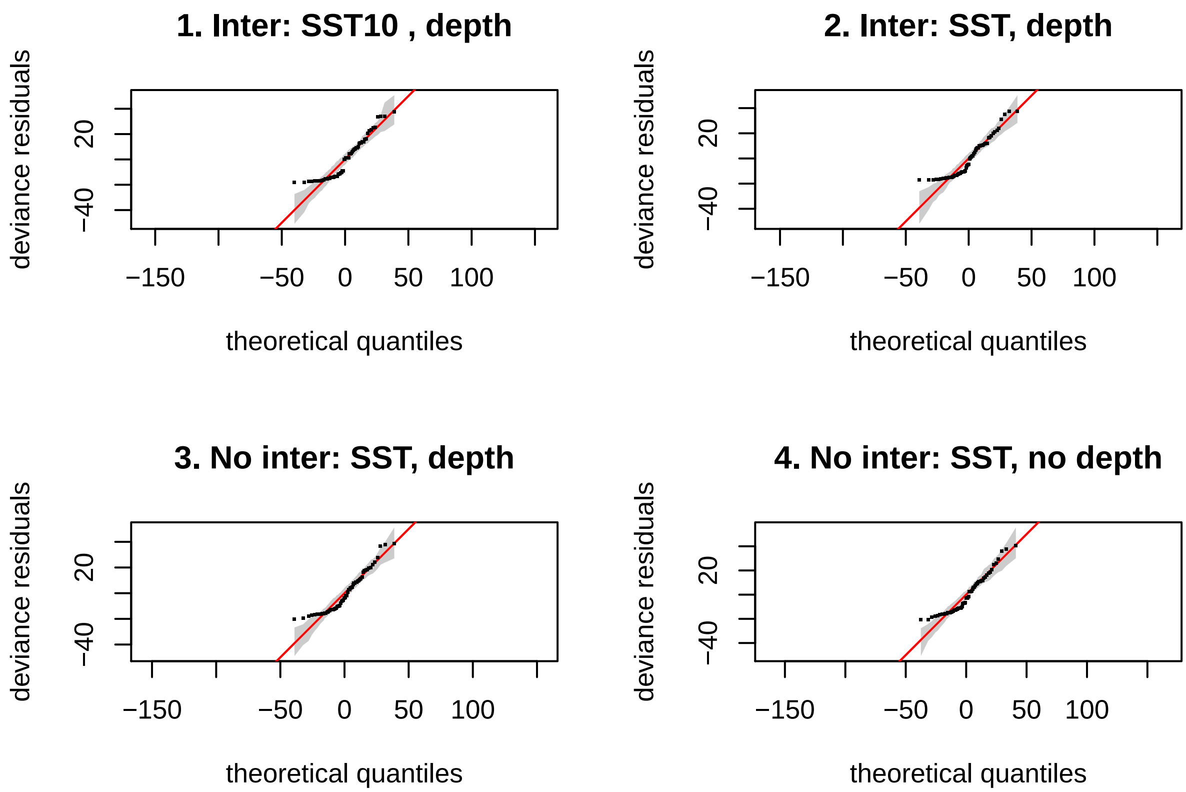

### Summary output for the group encounter rate model

```
##
## Family: Tweedie(p=1.384)
## Link function: log
##
## Formula:
## abundance.est ~ s(x, y, YearF, bs = "fs") + offset(off.set)
##
## Parametric coefficients:
##             Estimate Std. Error t value Pr(>|t|)
## (Intercept)  -5.1245     0.1778  -28.82   <2e-16 ***
## ---
## Signif. codes:  0 '***' 0.001 '**' 0.01 '*' 0.05 '.' 0.1 ' ' 1
##
## Approximate significance of smooth terms:
##                edf Ref.df     F  p-value
## s(x,y,YearF) 4.216     89 0.188 0.000717 ***
## ---
## Signif. codes:  0 '***' 0.001 '**' 0.01 '*' 0.05 '.' 0.1 ' ' 1
##
## R-sq.(adj) =  0.000871   Deviance explained = 8.05%
## -REML = 418.04  Scale est. = 18.006    n = 1899
```

Ideally, the residuals in the q-q plots should lie on a straight line and the figure below shows that there is some deviation, although less pronounced than the models for group size. Grey shaded areas show results of 100 replicates. The number shown in the individual plot caption is the model number (see Table 3); model number 3 was selected.

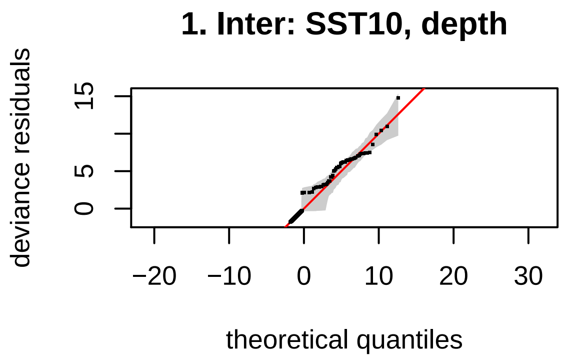
1. Inter: SST10, depth
deviance residuals
0
5
15
−20
−10
0
10
20
30
theoretical quantiles

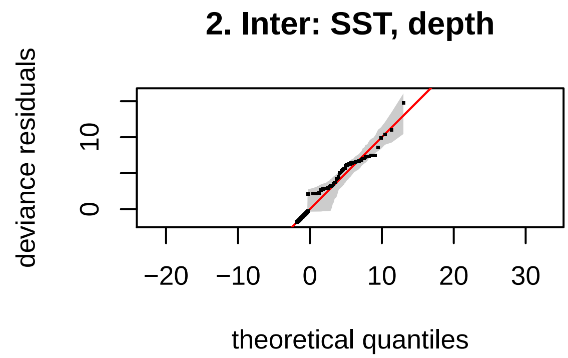
2. Inter: SST, depth
deviance residuals
0
10
−20
−10
0
10
20
30
theoretical quantiles

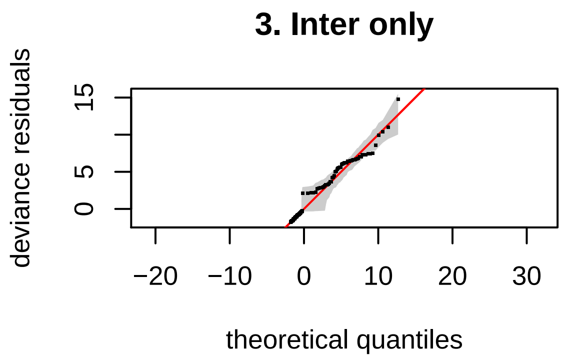
3. Inter only
deviance residuals
0
5
15
−20
−10
0
10
20
30
theoretical quantiles

## Appendix B: Estimated surfaces of BFT, number of groups and group size.

This appendix displays the surfaces of the estimated density of BFT for the extended region of interest (Figure B1), the estimated density of groups (Figure B2) and the estimated group sizes (Figure B3) and the corresponding CVs. The estimated numbers and average group sizes within block A are shown in Table 4.

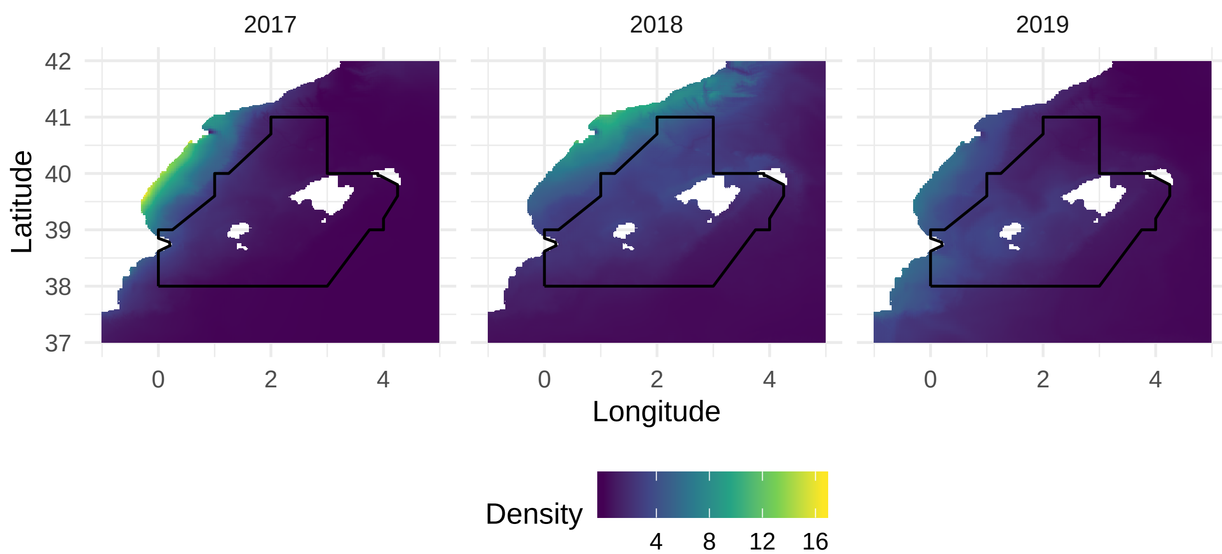


Figure B1. Estimated density of BFT (fish/km$^2$) for the extended region for 2017, 2018 and 2019. The CVs are shown in Figure 7.

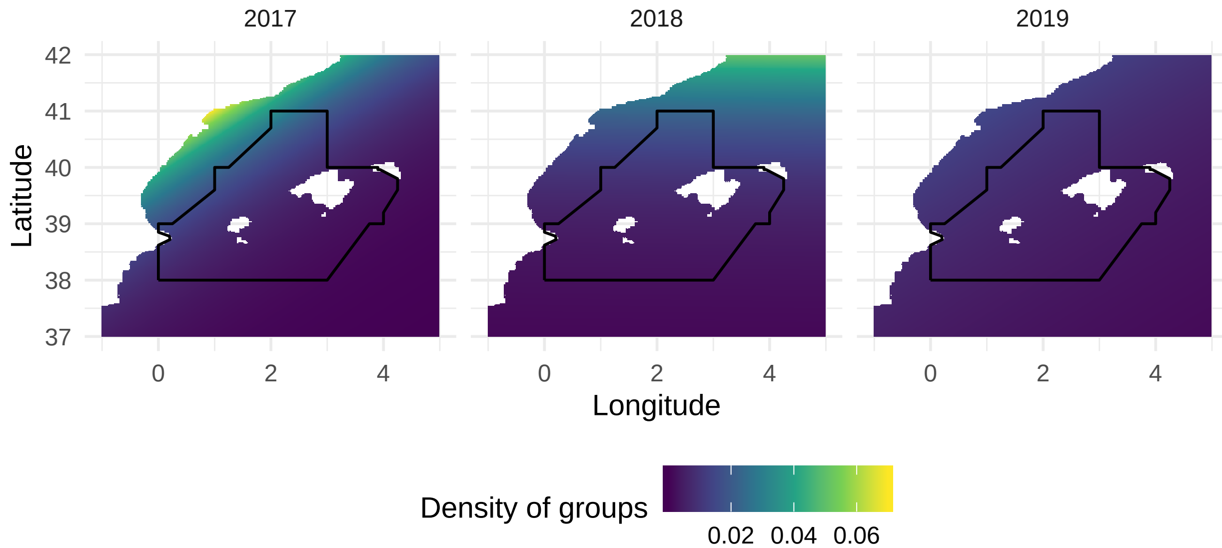
2017
2018
2019
42
41
40
39
38
37
Latitude
0
2
4
Longitude
Density of groups
0.02
0.04
0.06

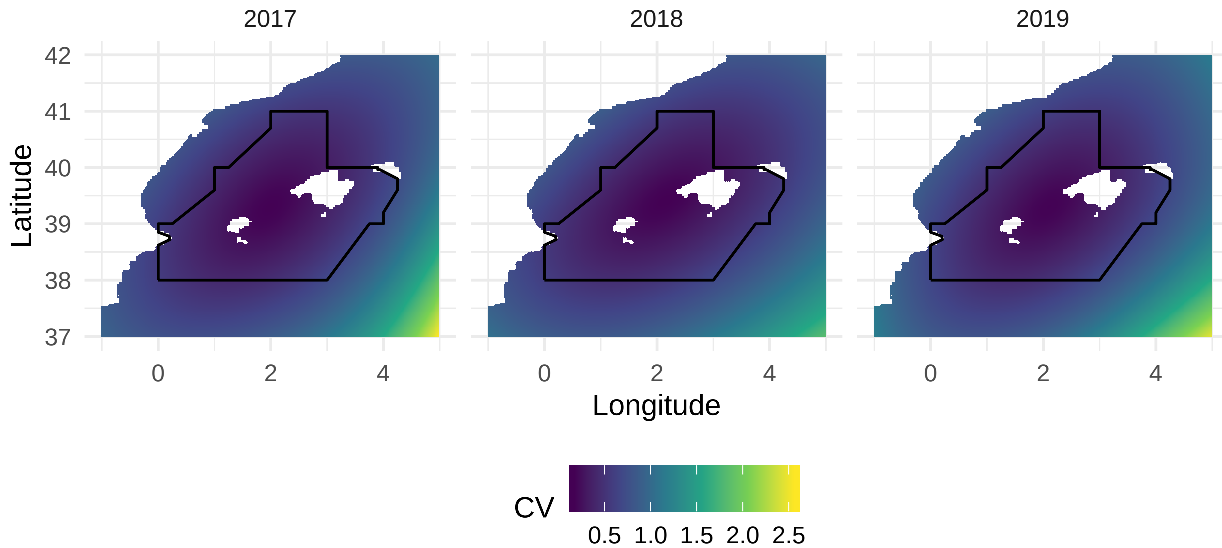


Figure B2. Estimated density of BFT groups (groups/km$^2$) and CV (not including detection function uncertainty) for 2017, 2018 and 2019.

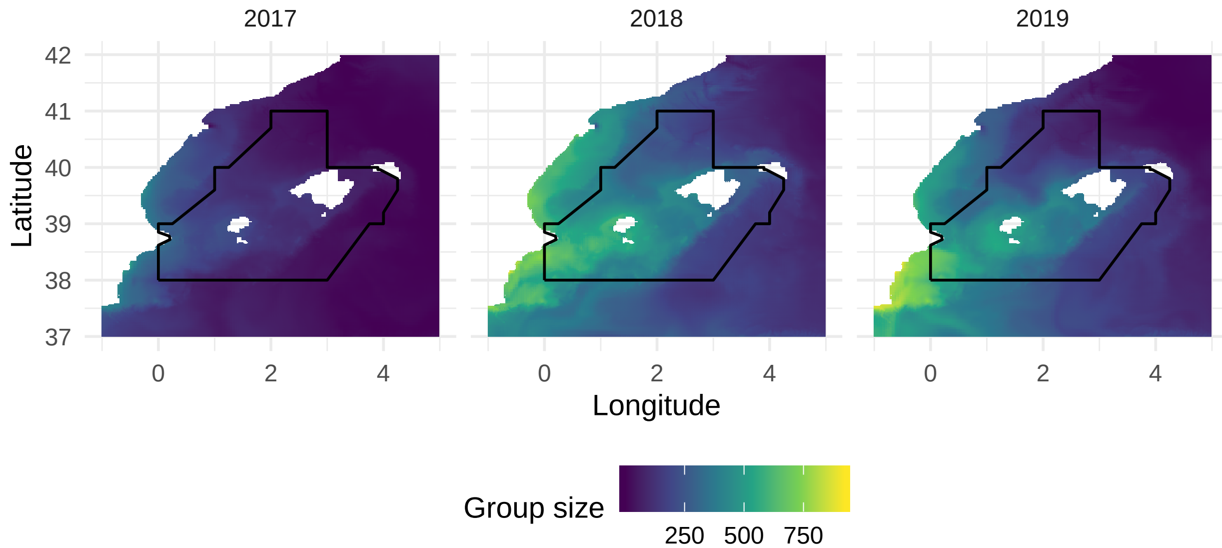

2017
2018
2019
42
41
40
39
38
37
Latitude
0
2
4
Longitude
Group size
250
500
750

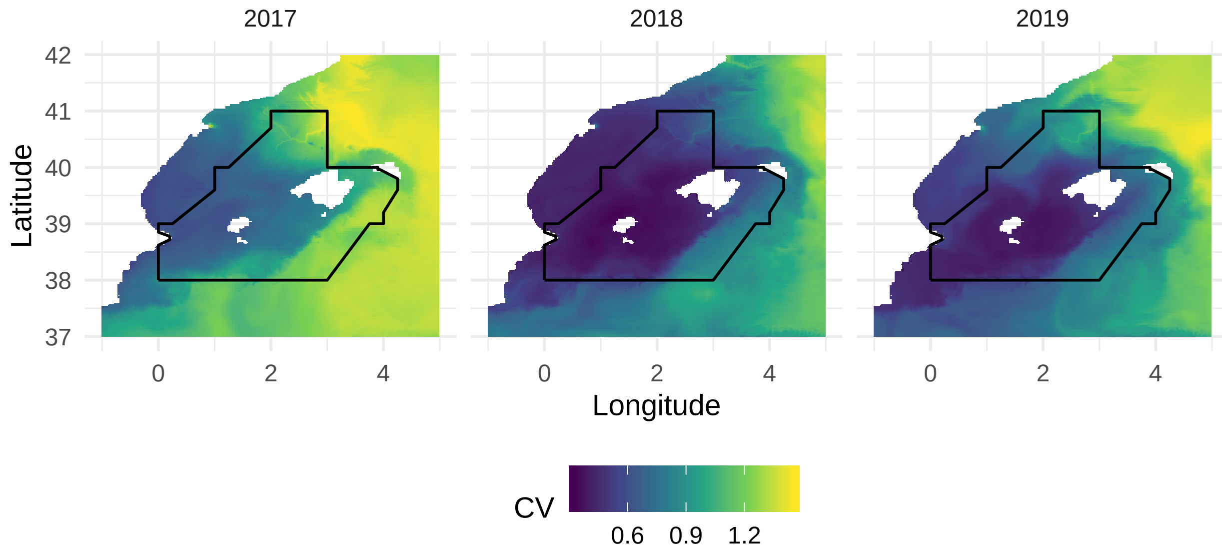


Figure B3. Estimated group sizes and CV using $SST$ on 10th June in 2017, 2018 and 2019.